Journal of Alloys and Compounds 788 (2019) 1021–1028

Contents lists available at ScienceDirect

Journal of Alloys and Compounds

journal homepage: http://www.elsevier.com/locate/jalcom

Hierarchy in nonlinear optical responses induced by metal cation tailoring effect in the In-containing chalcogenide compounds

Shichao Cheng [a], Xueyan Zhang [a], Ming-Hsien Lee [b], Jun Zhang [a, *]

[a] School of Physics Science and Technology, Xinjiang University, Urumqi, Xinjiang, 830046, China
[b] Department of Physics, Tamkang University, New Taipei, 25137, Taiwan

ARTICLE INFO

Article history:
Received 24 December 2018
Received in revised form
22 February 2019
Accepted 23 February 2019
Available online 25 February 2019

Keywords:
Density functional theory
Electronic structure
Nonlinear optical properties
Influence of cations

ABSTRACT

Factors controlling the nonlinear optical (NLO) responses of infrared materials remain unclear due to the complex systems spanning the whole main group elements and also transition elements. The microscopic mechanism of cation-affected optical properties is consequently necessary to the mid-infrared region. In this research work, the covalence, electronic structure and mechanism of nonlinear optical (NLO) responded for a typical IR system, In-containing chalcogenides with the formula $MInS_2$ (M = Ag, Li), are systemically investigated. It reveals that the orbitals hybridization, size effect and the cation electronegativity induce the changes of band gaps. Via tailoring the A-site cations, the microscopic factors affecting the optical band gap are analyzed. In addition to the effect of anionic groups on optical properties, we have found that the contributions of the A-site cations are not negligible. Furthermore, the electronic structures of sulfur in the compounds are susceptible to the type of cations, and consequently affect the NLO properties.

1. Introduction

Noncentrosymmetric materials are a fertile topic of research owing to the important physical properties that may be observed in many fields: pyroelectricity, ferroelectricity, piezoelectricity, or second harmonic generation (SHG) [1–6]. The second-order nonlinear optical (NLO) materials play an important role in laser science and technology [7–9]. Nowadays, numerous NLO crystals, such as KH_2PO_4 (KDP) [10], $KTiOPO_4$ (KTP) [11], β-Ba_2BO_4 (BBO) [12], LiB_3O_5 (LBO) [13] and $KBe_2BO_3F_2$ (KBBF) [14,15], are used in the visible and ultraviolet (UV)/deep ultraviolet (DUV) regions [16–22]. As for the middle and far infrared (IR) region [23,24], NLO crystals such as $AgGaQ_2$ (Q = S, Se) [25,26], $LiMQ_2$ (M = In, Ga; Q = S, Se) [27–29] and $ZnGeP_2$ (ZGP) [30] are commercially available. However, their application ranges are seriously hindered by inherent performance defects, such as low laser damage thresholds (LDTs) for $AgGaS_2$, harmful two photon absorption (TPA) at 1 μm for ZGP, and non-phase matching behavior (small birefringence) for $AgGaSe_2$. Therefore, the search for IR crystals [31,32] with good performance remains to be topics due to the crucial prerequisites of wide transparency, high laser damage thresholds and simple crystal growth [33]. And how to quantitatively and intuitively analyze the intrinsic relationship between NLO crystal performance and crystal structure characteristics [34] is still an open problem in the field of nonlinear optics.

Nowadays, the indium sulfide compounds have been widely used in the field of photoelectric material [35–37]. On the basic of investigation in the inorganic crystal structure database (ICSD), the compounds of $MInS_2$ (M = Li, Ag) [38,39] were found which belong to asymmetric space groups. As a I-III-VI ternary metal compound, $AgInS_2$ is widely used in the fields of photovoltaic cells, photocatalysis, optoelectronics and nonlinear optics due to its excellent optical properties. In recent years, the research of $AgInS_2$ quantum dots is a hot field [40–43]. In general, $AgInS_2$ crystals have two different polymorphs: tetragonal (chalcopyrite structure) and orthorhombic (wurtzite phase) [44]. The latter has shown more excellent photoelectrical and optical properties than that of chalcopyrite, and it has attracted much concentration. The simulated calculations of pure orthorhombic wurtzite $AgInS_2$ indicate that it is a direct bandgap semiconductor with a proper range of light absorption. Through investigation, the Li-containing compounds are mostly used in the battery field [45–47]. $LiInS_2$ is a new nonlinear chalcogenide biaxial material transparent from 0.4 to 12 μm that has been successfully grown in large sizes with good optical

* Corresponding author.
E-mail address: zhangjunxju@163.com (J. Zhang).

https://doi.org/10.1016/j.jallcom.2019.02.262
0925-8388/

qualities [48–51].

For these two compounds, they have the same [InS_4] groups, but their optical properties are significantly different. It is well known from the anionic group theory that the main contributions to the optical properties of the crystals are derived from the anionic groups [52]. Therefore, it is important to research the mechanism that the anionic groups are the same and while the properties are quite very different. In this work, the first principles method is adopted to study the electronic structures and optical properties of $AgInS_2$ and $LiInS_2$. The purpose of this work is to carry out a theoretical study of $MInS_2$ system with different cations and offer a proposal for the experiment researchers.

2. Computational details

The electronic structures and the optical properties of $MInS_2$ (M = Li and Ag) were calculated by using the density functional theory (DFT) [53] method implemented in the CASTEP package [54]. During the calculation, geometry optimization was performed using the BFGS minimization technique. The converged criterions for the geometry optimization include that the residual forces on the atoms, the displacements of atoms and the energy changes are less than 0.01 eV/Å, 5×10^{-4} Å, 5.0×10^{-6} eV/atom, respectively. After a series of successful tests, finally the generalized gradient-approximation (GGA) with Perdew-Burke Ernzerhof (PBE) functional was selected as the exchange-correlation potential [55]. Under the norm-conserving pseudopotential (NCP) [56], the following orbital electrons were treated as valence electrons: Li $2s^1$, Ag $4d^{10}5s^1$, In $4d^{10}5s^25p^1$, S $3s^23p^4$. The plane-wave energy cutoff of 850 eV for the electrons was chosen rationally, at the same time, a $2 \times 2 \times 2$ grid of Monkhorst-Pack mesh was used for k-point sampling. The other calculation parameters and convergent criteria were set by the default values of the CASTEP code.

The so-called length-gauge formalism derived by Aversa and Sipe [57] was adopted. At a zero frequency, the static second-order nonlinear susceptibilities can be ascribed to Virtual-Hole (VH) and Virtual-Electron (VE) [58,59]:

$$\chi^{(2)}_{\alpha\beta\gamma} = \chi^{(2)}_{\alpha\beta\gamma}(\mathrm{VE}) + \chi^{(2)}_{\alpha\beta\gamma}(\mathrm{VH})$$

The formulas for calculating the contributions from VE and VH are as follows:

$$\chi^{(2)}_{\alpha\beta\gamma}(\mathrm{VE}) = \frac{e^3}{2\hbar^2 m^3}\sum_{vcc'}\int\frac{d^3k}{4\pi^3}P(\alpha\beta\gamma)Im\left[P^{\alpha}_{vc}P^{\beta}_{cc'}P^{\gamma}_{c'v}\right]\left(\frac{1}{\omega^3_{cv}\omega^2_{vc'}} + \frac{2}{\omega^4_{vc}\omega_{c'v}}\right)$$

$$\chi^{(2)}_{\alpha\beta\gamma}(\mathrm{VH}) = \frac{e^3}{2\hbar^2 m^3}\sum_{vv'c}\int\frac{d^3k}{4\pi^3}P(\alpha\beta\gamma)Im\left[P^{\alpha}_{vv'}P^{\beta}_{v'c}P^{\gamma}_{cv}\right]\left(\frac{1}{\omega^3_{cv}\omega^2_{v'c}} + \frac{2}{\omega^4_{vc}\omega_{cv'}}\right)$$

Here, α, β, γ are Cartesian components; and v/v', c/c' denote valence bands (VBs) and conduction bands (CBs); And $P(\alpha\beta\gamma)$, ω_{ij} and P^{α}_{ij} refer to full permutation, the band energy difference and momentum matrix elements, respectively.

3. Result and discussion

3.1. Crystal structure and electronic structure

$LiInS_2$ (LIS) and $AgInS_2$ (AIS) which contain similar [InS_4] polyhedra are isostructural crystals and belong to the same space group $Pna2_1$ (No. 33) of the orthonormal system. The crystal structures of $MInS_2$ (M = Li and Ag) are shown in Fig. 1. When observed from the direction of the *b*-axis, the double [LiS_4] and [InS_4] tetrahedrons are alternately arranged in the *c* direction. In the *b*-*c* plane, the [LiS_4] and [InS_4] tetrahedrons form two layers – layer A and B which are alternately arranged. The structure of LIS is formed by [LiS_4] and [InS_4] tetrahedrons, and the S^{2-} ions are arranged in hexagonal packing with tetragonal and octahedral cavities (tetra and octahedron) [60]. The wurtzite structure of LIS and AIS is less dense than the chalcopyrite structure of $AgGaS_2$ due to the presence of empty cavities in the unit cell volume. Only half of the tetrahedra are occupied by lithium and indium ion while all octahedrons are empty. The unit cell parameters are roughly a = 6.8 Å, b = 6.9 Å, c = 8.1 Å for LIS, and a = 6.9 Å, b = 8.2 Å, c = 6.7 Å for AIS. The exact lattice parameters depend on the coloration, growth and annealing conditions and the exact stoichiometry, but the crystal structures of LIS and AIS are the same.

3.2. Electronic band structure

The band structures for title compounds are shown in Figs. 4 and 5. It is found that compounds LIS and AIS have direct energy band gap of 2.78 eV and 1.05 eV, respectively. While the optical experimental gaps for LIS and AIS are about 3.57 eV and 1.98 eV as reported [44,61]. The computational values are smaller than experimental gaps, and the small difference between the calculated and the experimental ones is because of the discontinuity of exchange correlation energy [62].

As shown in Fig. 2, the contributions at the top of valence bands (VBs) for the AIS are from the S 3*p* and Ag 4*d* states. The conduction bands (CBs) are similar for the isostructural compounds LIS (I) and AIS (II), which mainly come from In 5*s*, 5*p* and Li 2*s* states (for I) or Ag 4*p* states (for II), respectively. As for compound II, the VB near the Fermi can be divided into three regions: from −6 to −5 eV, the S 3*p* states overlap completely with the In 5*s* orbitals, showing strong In–S covalent interactions. The region from −4 to −2 eV is composed of Ag 4*d* and S 3*p* states, which make some contributions to the Ag–S bonds. Near the top of the VB (from −2 eV to Fermi), there is some obvious hybridization between Ag 4*d* and S 3*p* orbitals, revealing a few of chemical bonds between Ag–S. The bottom of CBs (1.5–8.0 eV) is dominated by the orbitals of In and S atoms. Accordingly, the [InS_4] units determine the energy band gap of compound II. For compounds I, In *s* and *p* states also contribute in the conduction band and very small difference between the Li 2*s* states make a few contributions in conduction bands for compound II. The atomic orbitals of these two crystals are shown in Fig. 3. The conduction band minimum (CBM) and valence band maximum (VBM) of AIS and LIS are mainly occupied by In and S atoms of the microscopic unit. Clearly, the band gap of AIS is determined by the interaction between In and S, but the Ag-S interaction plays a non-neglected role in the bandgap. Through the simulation calculation, we find that the band gap of the two compounds is different in the electronic track of the conduction band bottom. As show in Fig. S1, it can be clearly seen that at the bottom of the CBs of the compound AIS, the main contributions are from the In 5*s* orbital. But the compound LIS plays a major role in the bottom of the conduction band by the Li 2*s* orbital. Therefore, the role of Ag ions in the [InS_4] framework is that the conduction band portion is lowered to reduce the band gap [63].

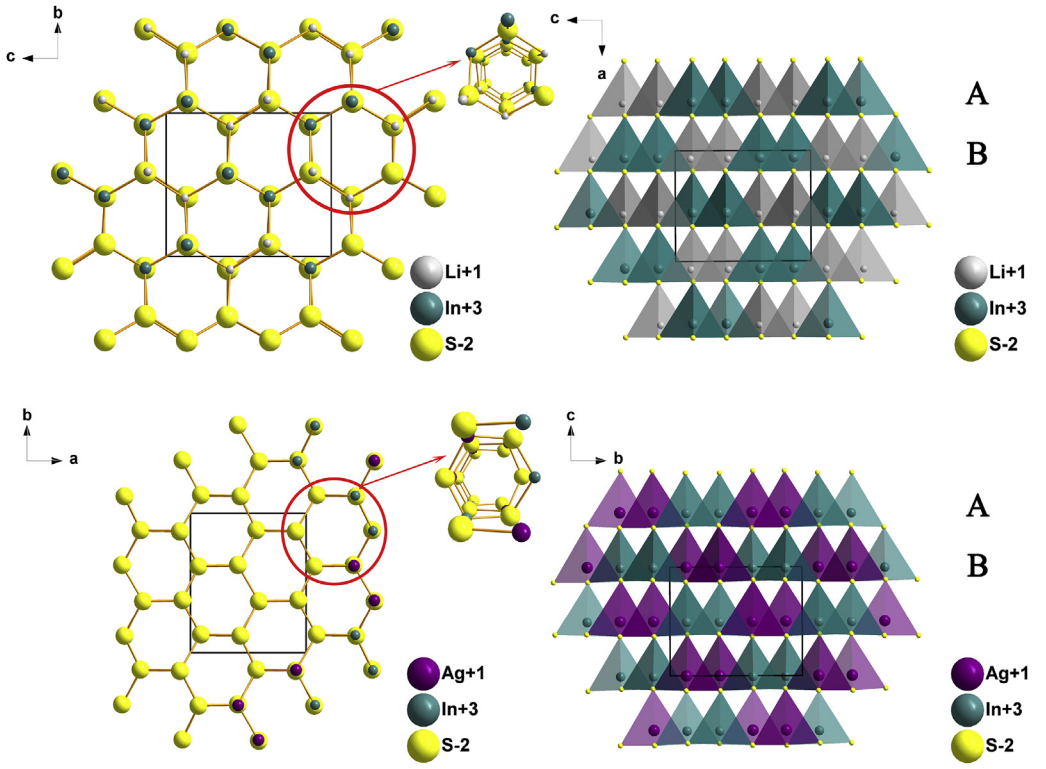

Fig. 1. Crystal structures of $LiInS_2$ and $AgInS_2$.

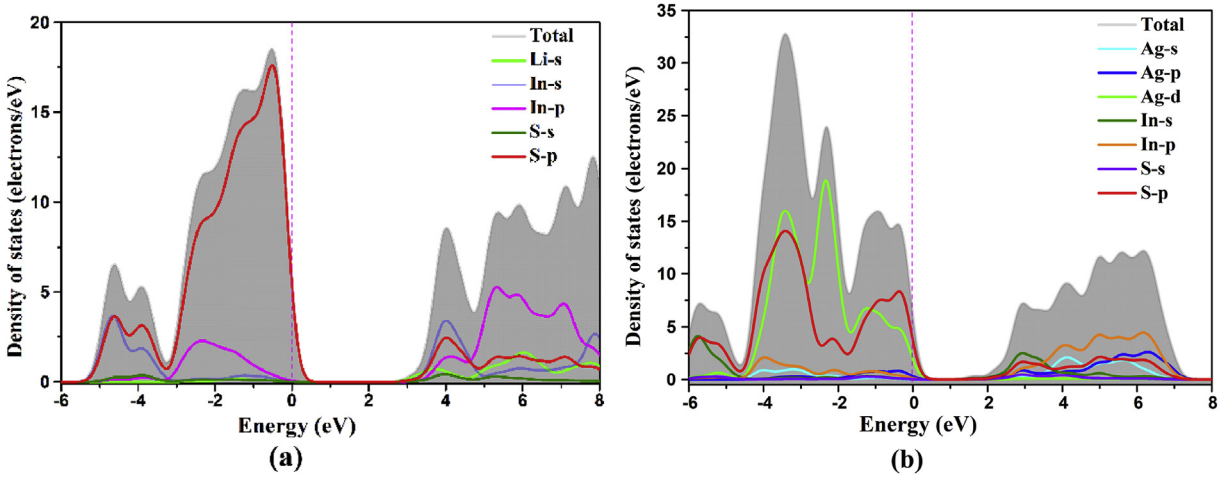

Fig. 2. Calculate partial densities of states of the LIS (a) and AIS (b).

The lithium is replaced by the larger electronegativity silver cations showing an increase in the DFT-calculated band gaps, which is consistent with the trend in optical gap observed by the experimental value. This hypothesis is supported by DFT calculations of the LIS and AIS lattice, as well as variations of the structure in which Li (Ag) cations are removed ([ ]InS_2), and Li (Ag) cations are replaced by Ag (Li) cations as shown in Figs. 4 and 5. In these calculations, we charge balance the loss of the cations by the addition of the corresponding number of electrons. In all three cases, the valence band is effectively pinned to the nonbonding S 3*p* states. Lithium is electropositive and thus it will not affect the positions dispersions of the valence and conduction band, illustrated by comparison of the band structures for ($LiInS_2$) and ([ ]InS_2). In contrast, removal of the Ag cations destabilizes the CBM due to the hybridization of the Ag 4*d* and S 3*p* states to form a manifold of antibonding states. However, the In−S interactions remain relatively unchanged across the $AgInS_2$ series due to the covalence of the [InS_4] tetrahedron units, and thus, the band gaps of the series are dictated the metal cations with different hybridizations in the valence band [64–66].

3.3. Enhancement mechanism of linear and nonlinear optical properties

The birefringence Δn and the contributions of atoms or groups to birefringence for LIS and AIS are listed in Table S3 and Fig. 6, together with the available experimental data for comparison [67].

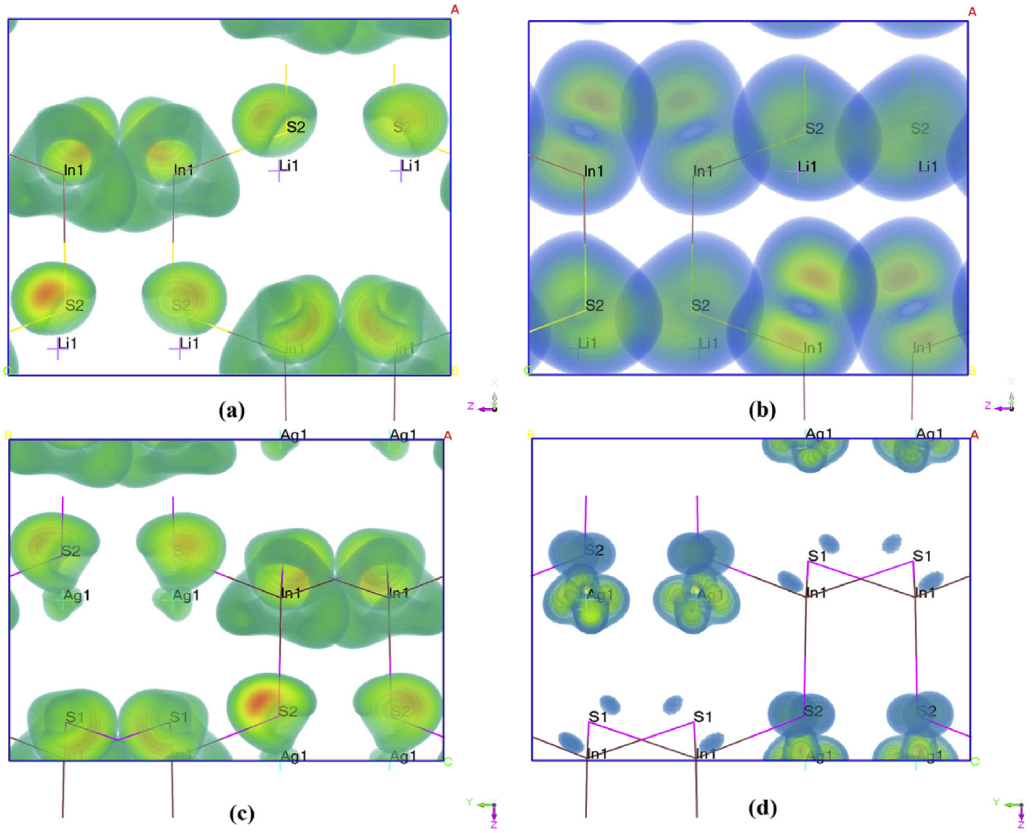

Fig. 3. Atomic orbitals of LIS (a, CBM; b, VBM) and AIS (c, CBM; d, VBM).

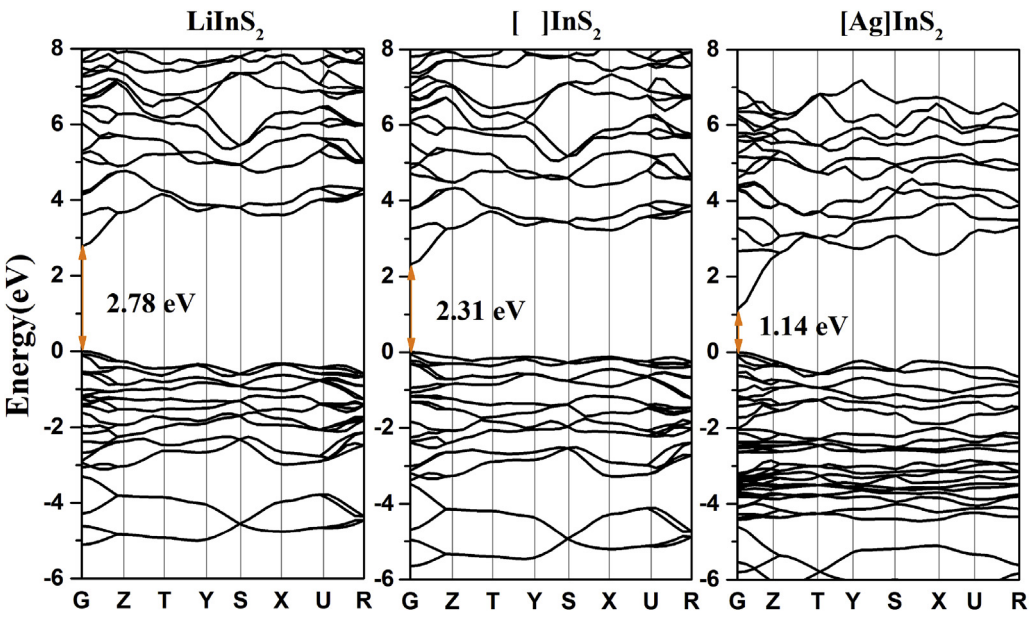

Fig. 4. Band structures of $LiInS_2$ and the structure of [ ]InS_2 in which the Li cations are removed, and [Ag]InS_2 in which the Li cations are replaced by Ag cations.

Here the birefringence of 0.013 and 0.061 @1064 nm for LIS and AIS was calculated by GGA + NCP which was also used to analyze the relationship between optical properties and crystal structure. In general, tetrahedral units are unfavorable to birefringence, however, the arrangement of [InS_4] in $AgInS_2$ is obviously distorted by the action of Ag [68,69]. Therefore, distorted [InS_4] groups are beneficial to optical anisotropy, which may one reason for the relatively large birefringence of AIS as compared to that of LIS. To further explore the source of birefringence, we calculate the response electron distribution anisotropy (REDA) index proposed by Yang et al. [70]. The response electron distribution anisotropy (REDA) approximation was proposed to analyze the relationship

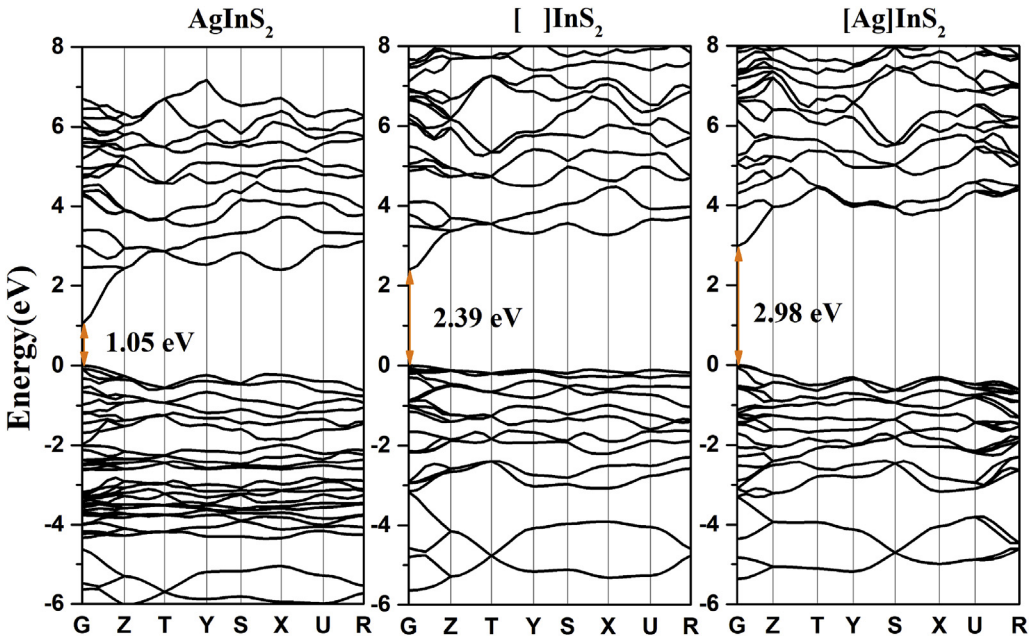

Fig. 5. Band structures of $AgInS_2$ and the structure of [ ]InS_2 in which the Ag cations are removed, and [Li]InS_2 in which the Ag cations are replaced by Li cations.

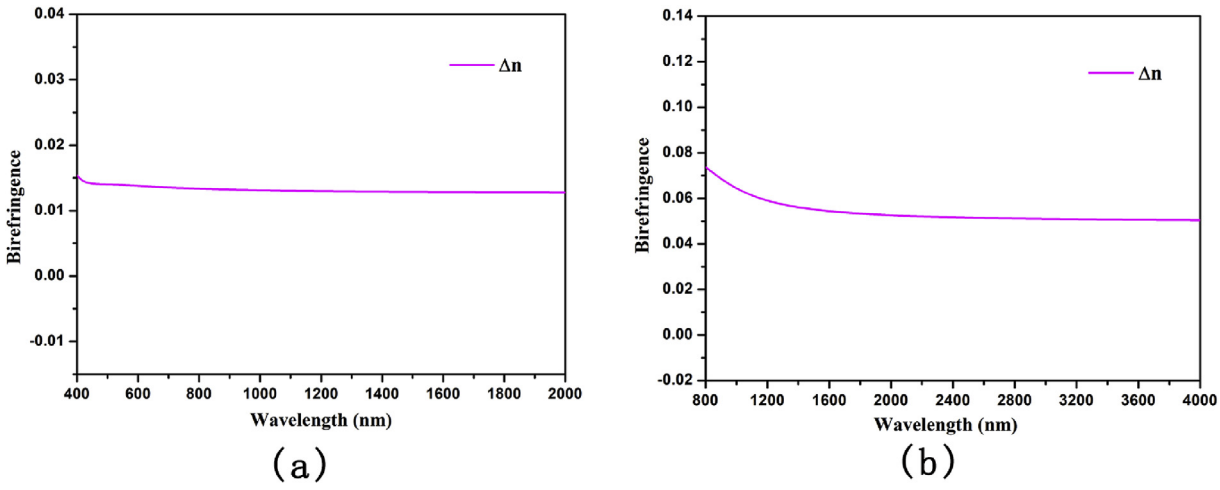

Fig. 6. Calculated birefringence of LIS (a) and AIS (b).

between optical anisotropy and distribution of bonding electrons in compounds. The result shows that the REDA index of In-S groups is 2.034, which has a larger value than Ag-S groups (1.047) in AIS. According to the results, the [InS_4] groups have more comparative contributions to birefringence than that of Ag-S groups in AIS. However, there are small contributions observed from [InS_4] groups in LIS. In consideration of the atomic volumes of A-site cations in these two compounds, they are quite different. Therefore, the volume action of Ag ions leads to an increase in the degree of [InS_4] polyhedral distortion, resulting in large optical anisotropy and then enhance the birefringence of AIS [71].

As of these two compounds belong to the asymmetric space groups, which is the most fundamental precondition of exhibiting SHG responses [72–74]. Through the first-principles methods, the calculated SHG coefficients of compounds I and II are listed as Table S2. To demonstrate the contributions of each atom in the SHG processes in real space, we also used SHG-density method. It should be noticed that the two virtual transition processes, namely virtual electron (VE) and virtual hole (VH) processes, contribute SHG process. From the band-resolved result [75] within the energy band framework which corresponds to individual electronic states of SHG coefficients, the contributions of the VE processes and VH processes are 62.80% and 37.20% to maximal SHG tensor for AIS, 75.84% and 24.16% for LIS. Therefore, VE processes are extremely predominant. SHG densities of VE processes are analyzed. Fig. 7 shows density of the SHG effect of occupied and unoccupied states of AIS and LIS.

The SHG coefficient of two compounds were also obtained based on DFT calculations [76]. There are three nonzero components of the second-order polarizability tensor, namely $d_{31} = d_{15}$, $d_{32} = d_{24}$ and d_{33} due to the symmetry of two compounds [77]. The non-vanishing independent SHG tensor $d_{15} = 4.43$ pm/V, $d_{24} = 4.57$ pm/V and $d_{33} = 10.07$ pm/V for AIS was calculated. The calculated SHG results are comparable to those of typical Cd-containing compounds [78]. As mentioned by Yang et al. [79], for the quality factors Q in IR NLO systems, SHG should larger than 10 KDP

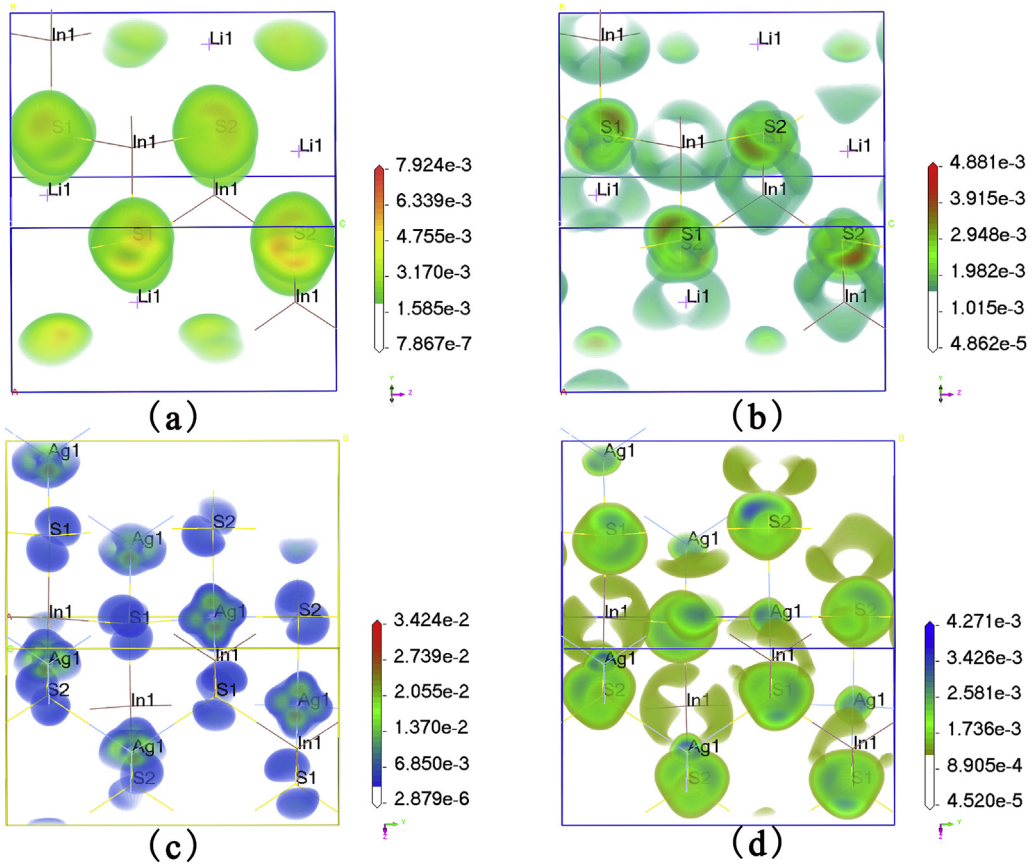

Fig. 7. SHG-density of LIS (a, occupied states; b, unoccupied states) and AIS (c, occupied states; d, unoccupied states).

($d_{36} = 0.39$ pm/V). Therefore, the title compounds satisfied this condition that have excellent genes that produce strong SHG response [80–82]. In addition, the SHG-density technique is applied to analyze the contributions of NLO-active units for the SHG effect [83]. Fig. 7 shows the SHG density of the virtual-electron (VE) transition process. It clearly shows that the Ag atoms play an important role in the occupied states. Besides, S atoms also make some contributions to SHG in the occupied states. Obviously, the Ag and S atoms make major contributions to the unoccupied states [84], the *sp* hybridization between S atoms and Ag atoms also contributes to SHG effect [85]. As for LIS compound, the S atoms play an important role in the occupied states. The occupied and unoccupied SHG density indicates that not only the [InS_4] groups have contributions to SHG effect, but also the contributions of lithium are appreciable and not negligible.

4. Conclusions

In this work, to distinguish the gap-determination factor and NLO active factor, two compounds $LiInS_2$ (LIS) and $AgInS_2$ (AIS) are studied using the Density Functional Theory. Via tailoring the A-site cations, it is found that the profound *d*-orbitals of the silver atom locate at the top of the VB, but the contributions of the lithium orbitals to the band-gap edge are very small. At the bottom of CB, the lithium orbitals contributions bring decisive role. Obviously, the silver *d*-orbitals in the Ag-containing crystals elevate the energy position of the VB relative to the CB, which make the band gaps narrower in these crystals. Through the simulation calculation, we find that effected of the cations on the anionic framework affects the optical properties of the material. It guides that the design and synthesis of compounds with excellent performance.

Acknowledgments

This work is supported by the National Natural Science Foundation of China (Grant No.11564038). MHL is grateful for the database service provided by NCHC (Taiwan) and computer equipment donated by KeyWin Inc.

Appendix A. Supplementary data

Supplementary data to this article can be found online at https://doi.org/10.1016/j.jallcom.2019.02.262.

References

[1] J.S. Knyrim, P. Becker, D. Johrendt, H. Huppertz, A new non-centrosymmetric modification of BiB_3O_6, Angew. Chem. Int. Ed. 45 (2006) 8239–8241.
[2] M. Luo, Y.X. Song, C.S. Lin, N. Ye, W.D. Cheng, X.F. Long, Molecular engineering as an approach to design a new beryllium-free fluoride carbonate as a deep-ultraviolet nonlinear optical material, Chem. Mater. 28 (2016) 2301–2307.
[3] T.T. Tran, H.W. Yu, J.M. Rondinelli, K.R. Poeppelmeier, P.S. Halasyamani, Deep ultraviolet nonlinear optical materials, Chem. Mater. 28 (2016) 5238–5258.
[4] S. Lee, H. Jo, K.M. Ok, $Bi_2Te_2O_6(NO_3)_2(OH)_2(H_2O)$: a layered bismuth tellurium nitrate hydroxide with multiple noncentrosymmetric chromophores, J. Solid State Chem. 271 (2019) 298–302.
[5] K.M. Ok, E.O. Chi, P.S. Halasyamani, Bulk characterization methods for non-centrosymmetric materials: second-harmonic generation, piezoelectricity, pyroelectricity, and ferroelectricity, Chem. Soc. Rev. 35 (2006) 710–717.
[6] I.V. Solovyev, Magnetic structure of the noncentrosymmetric perovskites $PbVO_3$ and $BiCoO_3$: theoretical analysis, Phys. Rev. B 85 (2012) 054420–054426.
[7] A.L. Schawlow, C.H. Townes, Infrared and optical masers, Phys. Rev. 112 (1958) 1940–1949.
[8] P.A. Franken, A.E. Hill, C.W. Peters, G. Weinreich, Generation of optical

harmonics, Phys. Rev. Lett. 7 (1961) 118–119.
[9] T.H. Mainman, Stimulated optical radiation in ruby, Nature 187 (1960) 493–495.
[10] J.J. De Yoreo, A.K. Burnham, P.K. Whitman, Developing KH_2PO_4 and KD_2PO_4 crystals for the world's most power laser, Int. Mater. Rev. 47 (2013) 113–152.
[11] T.A. Driscoll, H.J. Hoffman, R.E. Stone, Efficient second-harmonic generation in KTP crystals, J. Opt. Soc. Am. B 3 (1986) 683–686.
[12] C.T. Chen, B.C. Wu, A.D. Jiang, G.M. You, A new type ultraviolet SHG crystal -β-BaB_2O_4, Sci. Sin. Ser. B 28 (1985) 235–244.
[13] C.T. Chen, Y.C. Wu, A.D. Jiang, B.C. Wu, G.M. You, R.K. Li, S.J. Lin, New nonlinear-optical crystal: LiB_3O_5, J. Opt. Soc. Am. B: Opt. Phys. 6 (1989) 616–621.
[14] C.T. Chen, Z.Y. Xu, D.Q. Deng, J. Zhang, G.K.L. Wong, B.C. Wu, N. Ye, D.Y. Tang, The vacuum ultraviolet phase-matching characteristics of nonlinear optical $KBe_2BO_3F_2$ crystal, Appl. Phys. Lett. 68 (1996) 2930–2932.
[15] Z.S. Lin, J. Lin, Z.Z. Wang, C.T. Chen, M.H. Lee, Mechanism for linear and nonlinear optical effects in LiB_3O_5, CsB_3O_5, and $CsLiB_6O_{10}$ crystals, Phys. Rev. B 62 (2000) 1757–1764.
[16] B.B. Zhang, G.Q. Shi, Z.H. Yang, F.F. Zhang, S.L. Pan, Fluorooxoborates: beryllium-free deep-ultraviolet nonlinear optical materials without layered growth, Angew. Chem. Int. Ed. 56 (2017) 3916–3919.
[17] X.F. Wang, Y. Wang, B.B. Zhang, F.F. Zhang, Z.H. Yang, S.L. Pan, CsB_4O_6F: a congruent-melting deep-ultraviolet nonlinear optical material by combining superior functional units, Angew. Chem. Int. Ed. 56 (2017) 14119–14123.
[18] Y. Wang, B.B. Zhang, Z.H. Yang, S.L. Pan, Cation-tuned synthesis of fluorooxoborates: towards optimal deep-ultraviolet nonlinear optical materials, Angew. Chem. Int. Ed. 57 (2018) 2150–2154.
[19] H.P. Wu, S.L. Pan, K.R. Poeppelmeier, H.Y. Li, D.Z. Jia, Z.H. Chen, X.Y. Fan, Y. Yang, J.M. Rondinelli, H.S. Luo, $K_3B_6O_{10}Cl$: a new structure analogous to perovskite with a large second harmonic generation response and deep UV absorption edge, J. Am. Chem. Soc. 133 (2011) 7786–7790.
[20] G.Q. Shi, Y. Wang, F.F. Zhang, B.B. Zhang, Z.H. Yang, X.L. Hou, S.L. Pan, K.R. Poeppelmeier, Finding the next deep-ultraviolet nonlinear optical material: $NH_4B_4O_6F$, J. Am. Chem. Soc. 139 (2017) 10645–10648.
[21] Z.Z. Zhang, Y. Wang, B.B. Zhang, Z.H. Yang, S.L. Pan, Polar fluorooxoborate, NaB_4O_6F: a promising material for ionic conduction and nonlinear optics, Angew. Chem. Int. Ed. 57 (2018) 6577–6581.
[22] X.Y. Dong, Q. Jing, Y.J. Shi, Z.H. Yang, S.L. Pan, K.R. Poeppelmeier, J. Young, J.M. Rondinelli, $Pb_2Ba_3(BO_3)_3Cl$: a material with large SHG enhancement activated by Pb-chelated BO_3 groups, J. Am. Chem. Soc. 137 (2015) 9417–9422.
[23] K. Wu, S.L. Pan, A review on structure-performance relationship toward the optimal design of infrared nonlinear optical materials with balanced performances, Coord. Chem. Rev. 377 (2018) 191–208.
[24] F. Liang, L. Kang, Z.S. Lin, Y.C. Wu, Mid-infrared nonlinear optical materials based on metal chalcogenides: structure–property relationship, Cryst. Growth Des. 17 (2017) 2254–2289.
[25] A.O. Okorogu, S.B. Mirov, W. Lee, D.I. Crouthamel, A.Y. Dergachev, K.L. Vodopyanov, N. Jenkins, V.V. Badikov, Tunable middle infrared down-conversion in GaSe and $AgGaS_2$, Opt. Commun. 155 (1998) 307–312.
[26] G. Boyd, H. Kasper, J. McFee, F. Storz, Linear and nonlinear optical properties of some ternary selenides, IEEE J. Quantum Electron. 8 (1972) 900–908.
[27] A.H. Reshak, S. Auluck, I.V. Kityk, Several features of nonlinear optical susceptibilities of $LiGaX_2$ (X=S, Se) ternary compounds, J. Alloys Compd. 473 (2009) 20–24.
[28] L. Isaenko, I. Vasilyeva, A. Merkulov, A. Yelisseyev, S. Lobanov, Growth of new nonlinear crystals $LiMX_2$ (M=Al, In, Ga; X=S, Se, Te) for the mid-IR optics, J. Cryst. Growth 275 (2005) 217–223.
[29] Z. Kish, A.S. Kanishcheva, V.B. Lazarev, Y.N. Mikhailov, Synthesis and crystal structure of lithium thioindate $LiInS_2$, Dokl. Akad. Nauk SSSR 280 (1985) 397–401.
[30] G.D. Boyd, E. Buehler, F.G. Storz, Linear and nonlinear optical properties of $ZnGeP_2$ and CdSe, Appl. Phys. Lett. 18 (1971) 301–304.
[31] K. Wu, B. Zhang, Z. Yang, S. Pan, New compressed chalcopyrite-like $Li_2Ba-M^{IV}Q_4$ (M^{IV} = Ge, Sn; Q = S, Se): promising infrared nonlinear optical materials, J. Am. Chem. Soc. 139 (2017) 14885–14888.
[32] K. Wu, Z. Yang, S. Pan, Na_2BaMQ_4 (M=Ge, Sn; Q=S, Se): infrared nonlinear optical materials with excellent performances and that undergo structural transformations, Angew. Chem. Int. Ed. 55 (2016) 6713–6715.
[33] L. Kang, M.L. Zhou, J.Y. Yao, Z.S. Lin, Y.C. Wu, C.T. Chen, Metal thiophosphates with good mid-infrared nonlinear optical performances: a first-principles prediction and analysis, J. Am. Chem. Soc. 137 (2015) 13049–13059.
[34] F. Liang, L. Kang, Z.S. Lin, Y.C. Wu, C.T. Chen, Analysis and prediction of mid-IR nonlinear optical metal sulfides with diamond-like structures, Coord. Chem. Rev. 333 (2017) 57–70.
[35] S. Higashimoto, T. Nakase, S. Mukai, M. Takahashi, Copper-indium-sulfide colloids on quantum dot sensitized TiO_2 solar cell: effects of capping with mercapto-acid linker molecules, J. Colloid Interface Sci. 535 (2019) 176–181.
[36] Y. Pan, X.Z. Yuan, L.B. Jiang, H.B. Yu, J. Zhang, H. Wang, R.P. Guan, G.M. Zeng, Recent advances in synthesis, modification and photocatalytic applications of micro/nano-structured zinc indium sulfide, Chem. Eng. J. 354 (2018) 407–431.
[37] Y.X. Huang, Z.H. Wang, Y. Jiang, S.J. Li, M. Wang, Y.S. Ye, F. Wu, M. Xie, L. Li, R.J. Chen, Conductivity and pseudocapacitance optimization of bimetallic antimony-indium sulfide anodes for sodium-ion batteries with favorable kinetics, Adv. Sci. 5 (2018) 1800613–1800624.
[38] A.A. Vaipolin, Y.V. Rud, I.V. Rozhdestvenskaya, Interatomic interaction aspect of phase transition in $AgInS_2$ crystals, Cryst. Res. Technol. 23 (1988) 337–341.
[39] G.D. Boyd, H.M. Kasper, J.H. McFee, Linear and nonlinear optical properties of $LiInS_2$, J. Appl. Phys. 44 (1973) 2809–2812.
[40] I.A. Mir, V.S. Radhakrishanan, K. Rawat, T. Prasad, H.B. Bohidar, Bandgap tunable AgInS based quantum dots for high contrast cell imaging with enhanced photodynamic and antifungal applications, Sci. Rep. 8 (2018) 9322–9333.
[41] M.A. Sunil, J. Nagaraju, G.M. Rao, Tuning the opto-electrical properties of $AgInS_2$ films prepared by two- step process, Surf. Interfaces 10 (2018) 45–49.
[42] S.H. Wang, H.J. Li, X.P. Sun, Y. Xu, Novel structure of $AgInS_2$ compound under high pressure: first principles calculations, Solid State Commun. 284–286 (2018) 20–24.
[43] B.M.M. May, S. Parani, O.S. Oluwafemi, Detection of ascorbic acid using green synthesized $AgInS_2$ quantum dots, Mater. Lett. 236 (2019) 432–435.
[44] J.L. Shay, B. Tell, L.M. Schiavone, H.M. Kasper, F. Thiel, Energy bands of $AgInS_2$ in the chalcopyrite and orthorhombic structures, Phys. Rev. B 9 (1974) 1719–1723.
[45] S.M. Zhang, J. Chen, T. Tang, Y.Z. Jiang, G.R. Chen, Q.N. Shao, C.H. Yan, T.J. Zhu, M.X. Gao, Y.F. Liu, H.G. Pan, A novel strategy to significantly enhance the initial voltage and suppress voltage fading of a Li- and Mn-rich layered oxide cathode material for lithium-ion batteries, J. Mater. Chem. A 6 (2018) 3610–3624.
[46] S.M. Zhang, H.T. Gu, T. Tang, W.B. Du, M.X. Gao, Y.F. Liu, D.C. Jian, H.G. Pan, Insight into the synergistic effect mechanism between the Li_2MO_3 phase and the $LiMO_2$ phase (M = Ni, Co, and Mn) in Li- and Mn-rich layered oxide cathode materials, Electrochim. Acta 266 (2018) 66–77.
[47] Y. Cao, Y.X. Yang, Z.H. Ren, N. Jian, M.X. Gao, Y.J. Wu, M. Zhu, F. Pan, Y.F. Liu, H.G. Pan, A new strategy to effectively suppress the initial capacity fading of iron oxides by reacting with $LiBH_4$, Adv. Funct. Mater. 27 (2017) 1700342–1700353.
[48] S.P. Wang, X.T. Tao, C.M. Dong, J. Liu, M.H. Jiang, Synthesis and properties of $LiInS_2$ polycrystalline materials, J. Synth. Cryst. 35 (2006) 1167–1171.
[49] J. Qiao, Q.J. Liang, S.P. Wang, X.X. Xiong, X.T. Tao, T. Dekorsy, Optimized seeded bridgman growth and temperature dependent THz optical properties of LiInS2 crystals, CrystEngComm (2019). https://doi.org/10.1039/c8ce02052c.
[50] A. Khan, M. Sajjad, G. Murtaza, A. Laref, Anion-cation replacement effect on the structural and optoelectronic properties of the $LiMX_2$ (M = Al, Ga, In; X = S, Se, Te) compounds: a first principles study, Z. Naturforsch. 73 (2018) 645–655.
[51] A. Arunkumar, P. Vijayakumar, M. Magesh, P. Ramasamy, E.N. Rao, S.V. Rao, A study on structural, compositional, microhardness and dielectric properties of $LiInS_2$ crystal, Mater. Res. Innovat. (2018) 1–10.
[52] C.T. Chen, Y.C. Wu, R.K. Li, The anionic group theory of the non-linear optical effect and its applications in the development of new high-quality NLO crystals in the borate series, Int. Rev. Phys. Chem. 8 (2008) 65–91.
[53] L.J. Sham, M. Schlüter, Density-functional theory of the energy gap, Phys. Rev. Lett. 51 (1983) 1888–1891.
[54] S.J. Clark, M.D. Segall, C.J. Pickard, P.J. Hasnip, M.I.J. Probert, K. Refson, M.C. Payne, First principles methods using CASTEP, Z. Kristallogr. 220 (2005) 567–570.
[55] J.P. Perdew, K. Burke, M. Ernzerhof, Generalized gradient approximation made simple, Phys. Rev. Lett. 77 (1996) 3865–3868.
[56] A.M. Rappe, K.M. Rabe, E. Kaxiras, J.D. Joannopoulos, Optimized pseudopotentials, Phys. Rev. B 41 (1990) 1227–1230.
[57] C. Aversa, J.E. Sipe, Nonlinear optical susceptibilities of semiconductors: results with a length-gauge analysis, Phys. Rev. B 52 (1995) 14636–14645.
[58] B.B. Zhang, M.H. Lee, Z.H. Yang, Q. Jing, S.L. Pan, M. Zhang, H.P. Wu, X. Su, C.S. Li, Simulated pressure-induced blue-shift of phase-matching region and nonlinear optical mechanism for $K_3B_6O_{10}X$ (X = Cl, Br), Appl. Phys. Lett. 106 (2015) 031906–031911.
[59] J. Lin, M.H. Lee, Z.P. Liu, C.T. Chen, Mechanism for linear and nonlinear optical effects in β-BaB_2O_4 crystals, Phys. Rev. B 60 (1999) 13380–13389.
[60] L. Isaenko, I. Vasilyeva, A. Yelisseyev, S. Lobanov, V. Malakhov, L. Dovlitova, J.-J. Zondy, I. Kavun, Growth and characterization of $LiInS_2$ single crystals, J. Cryst. Growth 218 (2000) 313–322.
[61] L.I. Isaenko, A.P. Yelisseyev, Recent studies of nonlinear chalcogenide crystals for the mid-IR, Semicond. Sci. Technol. 31 (2016) 123001–123024.
[62] M.K. Chan, G. Ceder, Efficient band gap prediction for solids, Phys. Rev. Lett. 105 (2010) 196403–196407.
[63] W. Bi, N. Louvain, N. Mercier, J. Luc, B. Sahraoui, Type structure, which is composed of organic diammonium, triiodide and hexaiodobismuthate, varies according to different structures of incorporated cations, CrystEngComm 9 (2007) 298–303.
[64] A.E. Maughan, A.M. Ganose, A.M. Candia, J.T. Granger, D.O. Scanlon, J.R. Neilson, Anharmonicity and octahedral tilting in hybrid vacancy-ordered double perovskites, Chem. Mater. 30 (2017) 472–483.
[65] B. Bashir, B.B. Zhang, S.L. Pan, Z.H. Yang, Combination of d^{10} -cations and fluorine anion as active participants to design novel borate/carbonate nonlinear optical materials, J. Alloys Compd. 758 (2018) 85–90.
[66] J.B. Huang, M. Mamat, S.L. Pan, Z.H. Yang, Hierarchical active factors to band gap and nonlinear optical response in Ag-containing quaternary-chalcogenide compounds, J. Solid State Chem. 239 (2016) 30–35.
[67] S.P. Wang, Q.J. Liang, X.T. Tao, T. Dekorsy, Optical properties and birefringence

in $LiInS_2$ in the terahertz frequency range, Opt. Mater. Express 4 (2014) 575–586.
[68] C.T. Chen, Y.C. Wu, R.K. Li, The development of new NLO crystals in the borate series, J. Cryst. Growth 99 (1990) 790–798.
[69] R.K. Li, On the anionic group approximation to the borate nonlinear optical materials, Crystals 7 (2017) 50–56.
[70] B.H. Lei, Z.H. Yang, S.L. Pan, Enhancing optical anisotropy of crystals by optimizing bonding electron distribution in anionic groups, Chem. Commun. 53 (2017) 2818–2821.
[71] B.H. Lei, Z.H. Yang, H.W. Yu, C. Cao, Z. Li, C. Hu, K.R. Poeppelmeier, S.L. Pan, Module-guided design scheme for deep-ultraviolet nonlinear optical materials, J. Am. Chem. Soc. 140 (2018) 10726–10733.
[72] I.V. Kityk, B. Sahraoui, Photoinduced two-photon absorption and second-harmonic generation in As_2Te_3-$CaCl_2$-$PbCl_2$ glasses, Phys. Rev. B 60 (1999) 942–949.
[73] I.V. Kityk, B. Sahraoui, Infrared-induced nonlinear optical effects in chalcogenide glasses, J. Chem. Phys. 114 (2001) 8105–8112.
[74] K. Iliopoulos, D. Kasprowicz, A. Majchrowski, E. Michalski, D. Gindre, B. Sahraoui, Multifunctional $Bi_2ZnOB_2O_6$ single crystals for second and third order nonlinear optical applications, Appl. Phys. Lett. 103 (2013) 231103–231107.
[75] M.H. Lee, C.H. Yang, J.H. Jan, Band-resolved analysis of nonlinear optical properties of crystalline and molecular materials, Phys. Rev. B 70 (2004) 235110–235120.
[76] B. Sahraoui, R. Czaplicki, A. Klöpperpieper, A.S. Andrushchak, A.V. Kityk, Ferroelectric $AgNa(NO_2)_2$ crystals as novel highly efficient nonlinear optical material: phase matched second harmonic generation driven by a spontaneous and electric field induced polarizations, J. Appl. Phys. 107 (2010) 113526–113534.
[77] B. Sahraoui, I.V. Kityk, Mid-infrared light-induced second-harmonic generation in specific glasses, J. Optic .A Pure Appl. Optic. 5 (2003) 174–179.
[78] B. Derkowska, Z. Essaidi, B. Sahraoui, A. Marasek, F. Firszt, M. Kujawa, Nonlinear optical properties of $Zn_{1-x}Mg_xSe$ and $Cd_{1-x}Mg_xSe$ crystals, Opt. Mater. 31 (2009) 518–522.
[79] Z.H. Yang, C. Hu, M. Mutailipu, Y.Z. Sun, K. Wu, M. Zhang, S.L. Pan, Oxyhalides: prospecting ore for optical functional materials with large laser damage thresholds, J. Mater. Chem. C 6 (2018) 2435–2442.
[80] I.V. Kityk, A. Majchrowski, J. Ebothe, B. Sahraoui, Nonlinear optical effects in $Bi_{12}TiO_{20}$ nanocrystallites embedded within a photopolymer matrix, Opt. Commun. 236 (2004) 123–129.
[81] S. Abed, M.S. Aida, K. Bouchouit, A. Arbaoui, K. Iliopoulos, B. Sahraoui, Nonlinear optical and electrical properties of ZnO doped Ni thin films obtained using spray ultrasonic technique, Opt. Mater. 33 (2011) 968–972.
[82] A. Zawadzka, P. Płóciennik, J. Strzelecki, Z. Łukasiak, B. Sahraoui, Photophysical properties of Alq_3 thin films, Opt. Mater. 36 (2013) 91–97.
[83] D.W. Hou, Z.H. Yang, S.L. Pan, Electronic, bond order, linear optical properties of series of alkalimetal P-O-P linkage borophosphates, J. Alloys Compd. 706 (2017) 589–595.
[84] B.H. Lei, Q.R. Kong, Z.H. Yang, Y. Yang, Y. Wang, S.L. Pan, Hierarchized band gap and enhanced optical responses of trivalent rare-earth metal nitrates due to (d–p)π conjugation interactions, J. Mater. Chem. C 4 (2016) 6295–6301.
[85] J.N. Cheng, M.H. Lee, J. Zhang, Cation substitution inducing gap changes and covalent interaction flexibility enhancing second harmonic generation responses in d^{10} metal chalcogenides, J. Alloys Compd. 768 (2018) 883–888.